# Defense Technical Information Center
## Compilation Part Notice

## ADP011180

TITLE: Thermal Analysis of a Carbon Fiber Rope Barrier For Use in the Reusable Solid Rocket Motor Nozzle Joint-2

DISTRIBUTION: Approved for public release, distribution unlimited

This paper is part of the following report:

TITLE: JANNAF Rocket Nozzle Technology Subcommittee Meeting [21st] Held in Cocoa Beach, Florida on March 27-30 2001

To order the complete compilation report, use: ADB272466

The component part is provided here to allow users access to individually authored sections of proceedings, annals, symposia, etc. However, the component should be considered within the context of the overall compilation report and not as a stand-alone technical report.

The following component part numbers comprise the compilation report:
           ADP011179 thru ADP011182            ADP204752 thru ADP204783

# Thermal Analysis of a Carbon Fiber Rope Barrier For Use in the Reusable Solid Rocket Motor Nozzle Joint–2

J. Louie Clayton
National Aeronautics and Space Administration
Thermodynamics and Heat Transfer Group / ED25
Marshall Space Flight Center
Huntsville, Alabama

## Abstract

This study provides development and verification of analysis methods used to assess performance of a carbon fiber rope (CFR) thermal barrier system that is currently being qualified for use in Reusable Solid Rocket Motor (RSRM) nozzle joint-2. Modeled geometry for flow calculations considers the joint to be vented with the porous CFR barriers placed in the "open" assembly gap. Model development is based on a 1-D volume filling approach where flow resistances (assembly gap and CFRs) are defined by serially connected internal flow and the porous media "Darcy" relationships. Combustion gas flow rates are computed using the volume filling code by assuming a lumped distribution total joint fill volume on a per linear circumferential inch basis. Gas compressibility, friction and heat transfer are included in the modeling. Gas-to-wall heat transfer is simulated by concurrent solution of the compressible flow equations and a large thermal 2-D finite element (FE) conduction grid. The derived numerical technique loosely couples the FE conduction matrix with the compressible gas flow equations. Free constants that appear in the governing equations are calibrated by parametric model comparison to hot fire sub-scale test results. The calibrated model is then used to make full-scale motor predictions using RSRM aft dome environments. Model results indicate that CFR thermal barrier systems will provide a thermally benign and controlled pressurization environment for the RSRM nozzle joint-2 primary seal activation.

## List of Symbols

| | |
|---|---|
| A | normal surface area |
| C | specific heat |
| D | passage diameter |
| e | Euler constant |
| $f$ | Moody friction factor |
| $g_c$ | gravitational constant |
| GF | flow conductor |
| h | convective film coefficient |
| H | enthalpy |
| L | flow path length |
| M | molecular weight |
| m | mass |
| p | pressure |
| Q | heat rate |
| R | gas constant |
| T | temperature |
| U | internal energy |
| t | time |
| V | volume |
| W | work |
| x | coordinate direction |

### Greek

| | |
|---|---|
| $\Delta$ | difference operator |
| $\alpha$ | Darcy constant |
| $\rho$ | gas density |
| $\mu$ | gas viscosity |

### Subscripts

| | |
|---|---|
| g | gas |
| h | hydraulic |
| i | inlet |
| o | outlet |
| p | constant pressure |
| w | wall |
| v | constant volume |

## Introduction

Current manufacturing procedures used for close out of RSRM nozzle joint–2, Fig 1, involves injection of a room temperature vulcanizing silicon material (RTV) into the assembly gap after the joint has been bolted together. The assembly gap dimension is about 45 mils nominal and RTV injection penetration is usually inboard to the housing, full circumference of the joint.

---

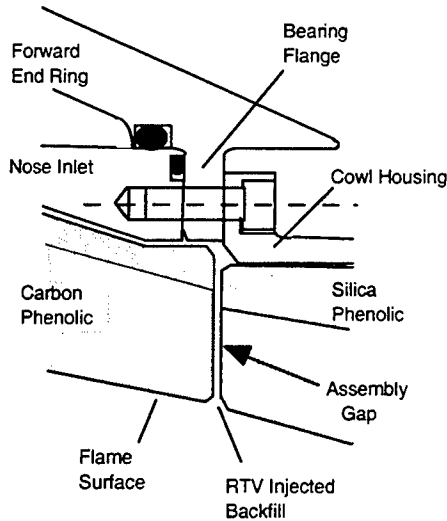* Approved for Public Release: Distribution is Unlimited

Fig 1- Current RSRM Nozzle Joint -2
Configuration

Due to structural deformations during pressurization of the motor, the assembly gap in the carbon phenolics open on the order of 10-20 mils with the largest deformation occurring at the flame surface. Typically the RTV backfill cannot track the deformation and fails to maintain a seal during motor operation. The result is an uncontrolled, hot gas pressurization of the joint free volume in the bearing vicinity (o-ring glands and bolt hole volumes). The exact nature of gas path geometry varies from confined and well-defined to large, circumferentially un-bonded areas. In general, if the gas path is more confined the local heating will be more severe.

The thermal problem with the current backfill process is the inherent randomness of the gas path geometry that is a result of process and hardware variation. The current back filling procedure results in gas path formation in virtually all motors (>90%) with resulting heat affected phenolics, adhesives and painted surfaces. Because of the peculiar sensitivity of heating severity to the gas path geometry, there exists a potential for exceeding the aluminum inlet and cowl housing reuse temperatures of 300°F.

Joint-2 has been analyzed thermally, Ref 1, by MSFC for worst case conditions and determined to be very robust in terms of thermal protection of primary and secondary seal. This particular metal housing design has several desirable features:

1. It is dynamically static which means the gland sealing surfaces remain essentially fixed when the motor pressurizes.
2. Metal to metal gaps leading to primary and secondary glands have a large (L/D) that serves to reduce the flow rate peak magnitude and provides significant cooling of the gas.
3. There is a large thermal capacitance at possible gas impingement points.
4. The joint does not have a large free volume available for pressurization.

Elimination of RTV and the use of a permeable CFR system in this joint will eliminate the random nature of gas path formation using the current procedure. This will allow for a controlled vented style pressurization of the joint free volume. In addition, compared to RTV backfill procedure, the CFR barrier system will be easier to use in terms of processing the joint and will result in a more streamlined assembly operation.

The following provides development and verification of analysis methods used to simulate the thermal performance of the CFR barrier system. Code development is derived from an existing base class of codes know as SINDA/JPR, Ref 2. Free constants that appear in governing equations are calibrated by parametric model comparison to hot fire, sub-scale test results. Finally, the calibrated model is then used to make full-scale motor thermal predictions using estimated RSRM aft dome environments.

## Model Development

Fundamentally, model development begins with derived class capabilities from the base SINDA/JPR computer code. This code was developed at MSFC for thermal analysis of the joint pressurization process associated with a single gas path connecting to an o-ring gland. The approach uses 1-D gas dynamic flow equations for the determination of conditions along the gas path and applies bulk formulated mass and energy equations to the volume filling process in an o-ring gland. Detailed heat transfer is simulated using the SINDA code, Ref 3, concurrently with the flow calculation routines embedded in the JPR code. Gas flow and heat transfer couplings (wall heat-transfer, film coefficient, flow enthalpies, etc.) are explicitly computed in time over the transient solution of the pressurization process. This loose coupling

allows the flow solution to be partitioned in time on a finer scale than solution to the conduction grid. The stiffness in the flow matrix, for typical joint filling situations, usually can be resolved with time steps on the order of 0.01-0.1 milliseconds; An inherent numerical property that is fixed by geometry, gas properties and typical rates of pressurization. The implicit solution of the thermal FE grid is usually stable at time steps one/two orders of magnitude larger than required for the flow thus an explicit "marching" numerical technique allows for a loosely coupled solution of flow and conduction matrices.

In JPR, the equations that describe flow along the gas path are formulated in terms of familiar R-C analogous "parallel" networks. Gas temperature and pressure relationships, are applied to the computational grid points, expressed in terms of (*resistance*) x (*potential difference*). The Darcy equation for compressible porous media flow can be simplified and cast in similar form and easily integrated into the existing JPR numerical scheme. Resistance contributions offered by the CFR are integrated into the overall system network resistance and simulated by the same nonlinear solution techniques used for convergence of the frictional internal flow resistances. JPR is numerically formulated as a point-to point solver (Gauss-Seidel) with partial back substitution.

As a result of the 1-D flow field associated with venting the joint symmetrically, the inlet normal flow areas, circumferential rope length and free volume available for pressurization are computed on a per unit depth basis. For this geometry, aspect ratios for flow and heat transfer calculations are similar to parallel flat plates. Hydraulic diameters that appear in the dimensionless heat transfer and flow relationships are assumed to be a function of gap dimension only. Porous media (Darcy) flow through the CFRs was also simplified via the 1-D assumption.

Geometry / Heat Transfer Modeling

Fig 2 provides a look at nozzle joint-2 configured with two CFRs in the assembly gap. This current design is referred to as the *dual face seal*.
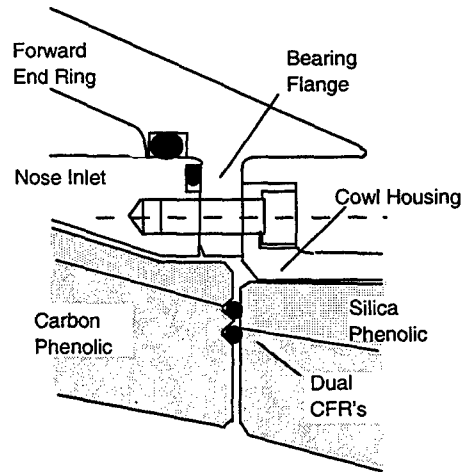


Fig 2 - Dual CFR Face Seal Nozzle Joint -2 Configuration

A thermal conduction finite element grid of the subject region, Fig 3, was constructed based on an idealized geometry. The grid is 2-D heterogeneous-anisotropic and contains approximately 4000 nodes and about 4200 isoparametric linear quad elements.
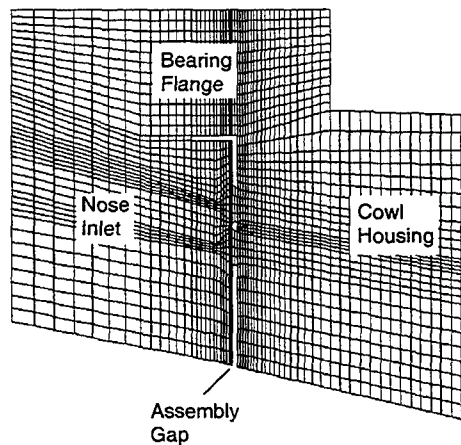


Fig 3 - 2-D Thermal Conduction Finite Element Grid of Nozzle Joint-2

Gas temperatures were calculated at 25 grid points along the flow path using a full up-winding scheme. These grid points were co-located with the FE nodes in the conduction grid. Convective boundary integrals were simplified to utilize a constant temperature distribution over the half element surfaces. The following detailed assumptions were applied to the FE grid and heat transfer modeling:

1. A simple 2-D grid (non-axisymmetric) was used because of the large radius of curvature relative to dimensions of the locally modeled region.
2. Material anisotropy was included for the carbon phenolics based on directional thermal conductivities for the given ply angle.
3. Material heterogeneity was simulated by variable property input as a function of temperature dependent char state. Char properties were used at temperatures above 1000°F.
4. Decomposition kinetics of the phenolic resins were not considered. The associated energies are typically small compared to sensible contributions of the advecting flow of the combustion gas.
5. Forced convective boundary conditions were applied along the assembly gap and through the CFR from inlet to stagnation points along the flex bearing. Effects of the hydrodynamic entry and variable gas properties were included.
6. Radiative loading (gas to wall) was not considered due to the small gap dimensions involved.
7. For the CFR, a non-equilibrium thermal situation exists for heat transfer, i.e., gas temperature not equal to solid media temperature. Nusselt relationships of the form:

$$\frac{\bar{h}}{D_h k} = Nu = C_1 Re^{0.5} Pr^{0.33} \qquad (1)$$

were applied on a volumetric basis where the constant $C_1$ was estimated from model calibration with test data.

8. Exponents for the dimensionless parameters in Eq (1) were inferred from relationships derived for packed bed heat transfer applicable to cylinders in a cross-flow.
9. For the Reynolds number evaluation, superficial gas velocities were used where the characteristic dimension was taken as the square root of the permeability.
10. At impingement points along the flow path, augmentation of the heat transfer rates was estimated using relationships found in Ref 4.
11. Variable gas specific heats were used in the nodal energy balance. Gas properties data were taken from Ref 5.

## Gas Flow Modeling

The flow network was 1-D and utilized a course descritization of the domain. Serial resistances were defined for the inlet, both CFR's, in-board portions of the assembly gap and metal gaps leading into the primary o-ring gland. Shown in Fig 4 is the basic arrangement of the network and locations of computed pressure points and assigned volumes.
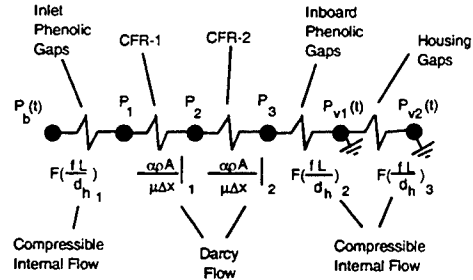


Fig 4 - 1-D Transient Internal / Darcy Flow Network

For test correlation, the flow model does not include the serial resistance offered by the primary o-ring metal gaps. These test, Ref 6, were conducted using an equivalent bulk volume appended to the end of a simulated joint-2 assembly gap.

## Basic Equations for Flow Calculations

Calculation of the thermodynamic state in the assigned volumes was based on a bulk formulation of the unsteady form of mass and energy conservation equations. They are specified as:

$$\frac{dm}{dt} = (\dot{m}_i - \dot{m}_o) \qquad (2)$$

$$\dot{Q} + H_i = \frac{d}{dt}(mU) + H_o + W \qquad (3)$$

where; $\dot{Q} = \bar{h}A(T_w - T_g)$

$\Delta U = C_v \Delta T$

$\Delta H = C_p \Delta T$

$pV = mRT \qquad (4)$

These equations are finite differenced by fully implicit methods and applied to the grid points capable of storing mass. At connect points along the assembly gap mathematical relationships for the primary variables are derived from the steady form of the conservation equations. From a functional standpoint, these relationships take the form of simple weighted averages where the

weight factors are the nonlinear conductance terms for the network, see Fig 4.

Derivation of conductance terms in the flow network is based on two separate methods of fluid transport: compressible-internal flow and porous media flow through the CFR's. In general, the computation boils down to the evaluation of an equation of the form:

$$GF_i = \frac{\dot{m}}{\Delta P} \qquad (4)$$

where the mass flow rate in numerator is computed by one of the following methods:

$$\dot{m} = p_i A \sqrt{\frac{g_c M}{eRT_i}} f\left(\frac{L}{D}, \frac{p_j}{p_i}\right) \qquad (5)$$

for internal flow, and

$$\dot{m} = \frac{\alpha \rho A}{\mu \Delta x}\left(P_i - P_j\right) \qquad (6)$$

for Darcy flow through the CFR. The weighted average formula applied to the grid points takes the transcendental form:

$$P_i = \frac{GF_{i-1}P_{i-1} + GF_iP_{i+1}}{GF_{i-1} + GF_i} \qquad (7)$$

The collection of weighted average formulas at the arithmetic grid points forms a system of non-linear simultaneous equations that are converged every iterative pass of the implicit solution to Eqs (2,3). This procedure may be termed "quasi-steady" from the standpoint of formulation of equations along the flow path. For gas flow modeling, the following detailed assumptions were made:

1. Bulk control volumes were assigned on a cubic inch per circumferential linear inch basis of joint free volume. All flow calculations were 1-D.
2. Temperature and equilibrium composition specific heats derived for the propellant combustion gases were used for enthalpy and internal energy terms.
3. The ideal gas law used equivalent molecular weights where volume contents are perfectly mixed. Total pressures were computed from the relationship.
4. Thermally dependent properties used in Darcy resistance were evaluated at a

CFR bulk mean temperature along the direction of flow. Porous media flow was assumed to be 1-D.

Model Calibration Procedure

Benchmarking for flow model calibration involved back fitting dynamic permeability to pressure trace data obtained from the Joint Environment Simulator (JES) series of tests, Ref 6. Internal flow losses were determined using standard textbook correlations; therefore, parametric optimization of "just" the permeability sufficed to give reasonable agreement with measured data. This outcome was considered likely due to the fact that the CFRs resistance controls the overall rate of gas flow into the joint.

Lab measured cold gas CFR permeability values were used for initializing the Darcy constant in the model. From observation of JES measured pressure response, several permeability dependences were discovered and incorporated. First was a sensitivity to initial gap size and hence initial squeeze on the CFR. At a minimum gap of 25 mils, the initial permeability was estimated to be $\sim 3 \times 10^{-10}$ in$^2$ and transitioned to $\sim 5 \times 10^{-9}$ in$^2$ at the maximum assembly gap of 65 mils. This effect was attributed to the mechanical deformation of the microstructure of the CFR under different levels of compressive load as a function of CFR squeeze. This shift in permeability causes a significant difference in $\Delta p$'s across the CFR for the various cases. A second dependency was observed in the form of a time based pressure lag in the measured data that could only be explained by the in-situ deposition of alumina ($Al_2O_3$) on the surface of the CFR during the transient. Permeability values had to be adjusted a full order of magnitude from the initial value over the fill transient. A simple accumulation model was devised to "dynamically" transition the permeability as a function of total deposition on the CFR surface. Post-test inspection shows significant alumina deposition on outboard surfaces of the CFR.

Also extracted from JES tests were gas temperatures useful in determination of system heat transfer rates. The convective heat transfer in the gaps is approximated well by standard internal flow correlations. For the CFR, temperature measurements were necessary to calculate the effective porous media volumetric heat transfer coefficients. Model development included the potential for a non-equilibrium gas-solid situation in the CFR as discussed in previous

sections. JES testing provided gas
temperature data for several cases and heat
transfer coefficient parametrics allowed for
back fitting predicted response to observed
gas temperatures.

The following section provides the calibrated
model results comparison to the JES
measured data.

## JES-3 Single CFR, 25 mil Gap

Shown in Fig 5 are model-calibrated results
for the JES-3 test. This case was a single
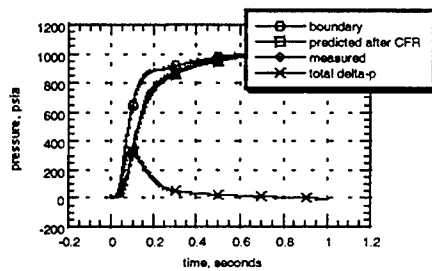CFR face seal configuration with the
minimum 25 mil assembly gap.



Fig 5 - JES-3 Single CFR Model Predicted
vs. Measured Pressures, 25 mil Gap

Predicted pressure response is in excellent
agreement with the measured values. Fill
times are on the order of ½ second and
pressure differentials of about 300 psi. Fig 6
shows the gas temperature comparisons for
this case.
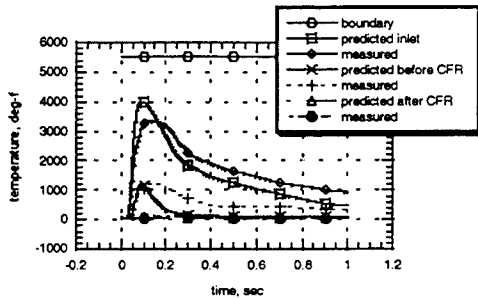


Fig 6 - JES-3 Single CFR, Model Predicted
vs. Measured Temperature, 25 mil
Gap

A constant boundary temperature of 5540°F
was imposed at time zero. Computed gas
temperatures at the inlet and in front of the
CFR were in good agreement with the
measured data. Differences in response
decay times are attributed to thermocouple
(TC) wall effects. Better comparison

agreement could be obtained by thermally
modeling the TC. The CFR backside gas
temperature increase was <10°F. This TC
measurement was present in all tests and
was used for calibration of the volumetric
heat transfer coefficient. The constant $C_1$
was adjusted until the desired backside $\Delta T$
was matched as a least squares best fit for
all tests in the series.

## JES-6 Dual CFRs, 25 mil Gap

Fig 7 provides a look at model predicted
pressures versus the measured data for the
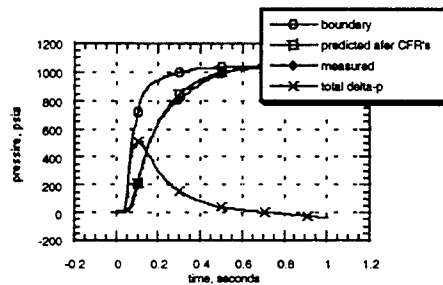dual CFR face seal at the minimum
assembly gap.



Fig 7 - JES-6 Dual CFR Model Predicted
vs. Measured Pressures, 25 mil
Gap

Again, the comparison shows very good
pressure response agreement. Fill times
(about 0.7 second) and total pressure
differentials (about 450 psi) have increased
over the single CFR case primarily due to
doubling of the flow path resistance. Fig 8
shows the computed gas temperatures
versus measured for the gap region
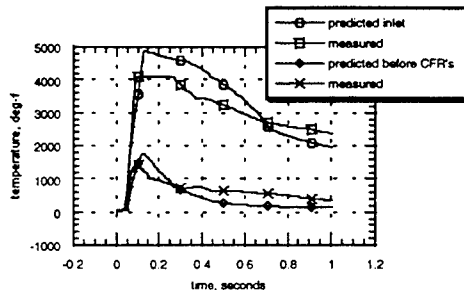outboard of CFRs (the inlet).



Fig 8 - JES-6 Dual CFR Model Predicted
vs. Measured Inlet Temperatures, 25
mil Gap

194

Inlet temperature comparison is acceptable. Peak measured inlet temperatures saturated the type-K thermocouple at 4100°F with the model prediction closer to 5000°F. Gas temperatures in front of CFRs are in the 1500-1700°F range. Fig 9 shows the gas temperature results for in-between and after the CFRs.
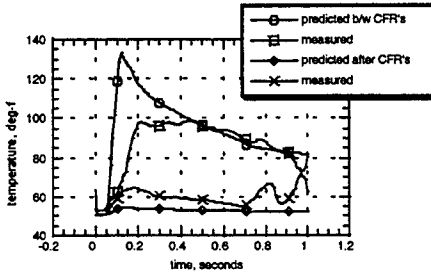


Fig 9 - JES-6 Dual CFR Predicted vs. Measured Temperatures, 25 mil Gap

For this case, measured gas temperatures between the CFRs increased about 50°F and backside temperature increase was <10°F. Model results compare well globally considering the overall range of computed temperatures in the model.

JES-6, Dual CFRs, 65 mil Gap

Fig 10 provides a look at model predicted pressures versus the measured values for a dual CFR system configured at the maximum assembly gap of 65 mils.
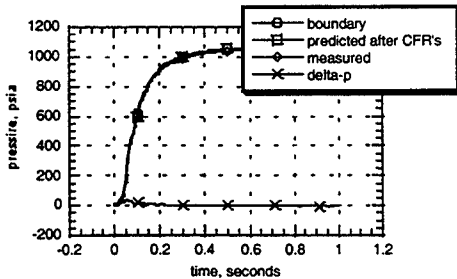


Fig 10 - JES-6 Dual CFR Model Predicted vs. Measured Pressures, 65 mil Gap

Model and measured pressures are in very good agreement for this case. For the large assembly gap, joint volume filling essentially follows chamber filling with little and/or no discernable fill time associated with the event. Pressure differentials are < 60 psi. Fig 11 shows the gas temperature comparisons for this case.
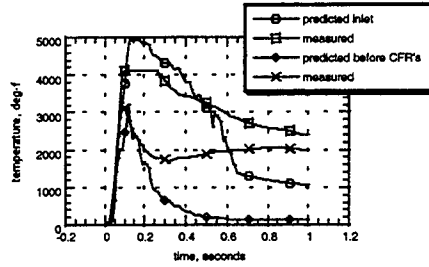


Fig 11 - JES-6 Predicted vs. Measured Temperatures Before CFRs in the Inlet Region, 65 mil Gap

There is very little gas sensible energy loss from chamber to inlet regions outboard of the CFR for this case. Temperatures are on the order of the 3000°-5000°F. Adjacent to the CFR, temperatures are considerably hotter than the minimum gap results due to higher peak flow rates (higher input heat rate) and wall heat transfer is less due to increased gap hydraulic diameter.
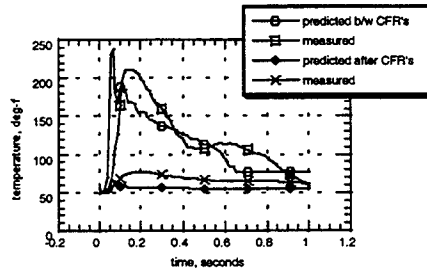


Fig 12 - JES-6 Predicted vs. Measured Temperatures Between and After CFRs, 65 mil Gap

For the larger gap spacing, in-between CFR gas temperatures can increase as much as ~160°F over start conditions. Temperature increase after the CFRs is approximately 20°-30°F. Again, model predictions are in fair agreement given overall magnitudes of the globally computed temperatures.

Flight Support Motor (FSM)-9 Assembly Gap Bounding Case

Predicted pressures for FSM-9 static test Joint-2 Dual CFR face seal are shown in Fig 13. For this case, the potential variation in volume filling transient is depicted by the shaded gray area where the boundaries are defined by results generated by max/min assembly gaps. Results indicate a fill time variation of about 0.2 second with the quicker times occurring with larger gaps. Inferring a nominal response from Fig 13

195

would indicate joint filling is complete at about 0.6 second.
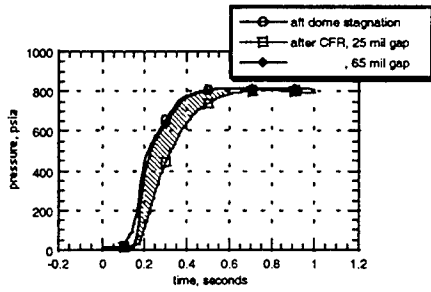


Fig 13 - FSM-9 Predicted Pressures

Joint-2 gas temperature predictions for FSM-9 are provided in Figs 14-16. Fig 14 shows that, as a function of assembly gap, inlet gas temperatures adjacent to the CFR range from 1800°-4000°F. A nominal estimation (45 mil gap) would be in the 2500°-3000°F range.
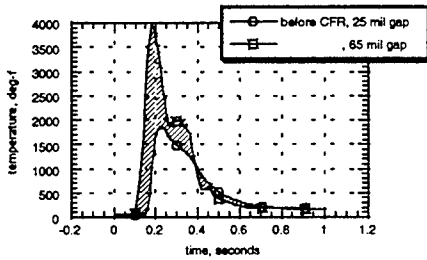


Fig 14 - FSM-9 Predicted Gas Temperatures in Assembly Gap Before CFRs

There is a significant reduction in temperature across the first CFR regardless of gap size. In-between temperatures are shown in Fig 15. Predicted variation in gas temperature increase, for this location, range from 60°F < $\Delta T$ < 350°F, depending on local gap.
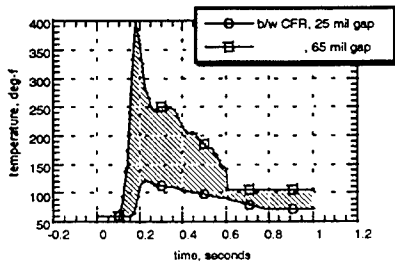


Fig 15 - FSM-9 Predicted Gas Temperatures in Assembly Gap Between CFRs

Fig 16 shows predicted temperatures for gasses that exit the in-board CFR and are headed for joint volumes. The effect of assembly gap variation on temperature magnitude has diminished to the point of inconsequential in terms of heating. Predicted variation in temperature increase for this location is about 3° < $\Delta T$ < 30°F.
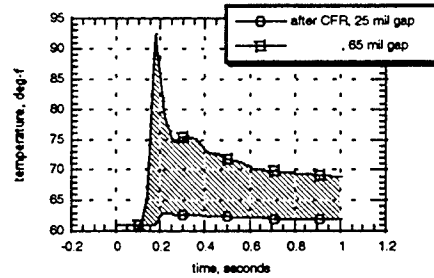


Fig 16 - FSM-9 Predicted Gas Temperatures in Assembly Gap After CFRs

Conclusions

The RSRM nozzle joint-2 CFR barrier system is predicted to perform in FSM-9 in a similar manner as demonstrated by JES model validation testing. This conclusion is based on the following considerations. JES test environments, i.e., ignition pressure rise rate, gas temperature and composition are similar to full-scale motor environments; thus, there is no issue with thermal boundary conditions. Further, the JES testing had a reasonable amount of geometric and kinematical similarity to full-scale hardware. The 1-D flow assumptions are approximately valid for a pressurization event of this joint. Circumferential flow can be addressed by steady Computational Fluid Dynamics (CFD) analyses if needed. Lumping of volumes in the test, to account for a more distributed situation in the full-scale hardware, is adequate if the controlling flow path resistance is the CFRs. This is believed to be the case based on the known "as-built" hardware housing gaps and overall assembly variation. Dynamic gap opening was not simulated in the JES test but was included in the FSM-9 model predictions. If the CFRs remain intact and seated, results indicate this effect is minimal in terms of gas temperature increase inboard of the barriers.

As a result of model calibration observations and review of the test data, the following general conclusions are drawn:

1. The excellent observed CFR thermal performance exploits the fact that the joint is vented. Pressurization rates for the free volumes behind the rope are rapid and total volume filling occurs by the time the chamber pressure trace is essentially neutral.

2. Another beneficial aspect of the CFRs is the filtering of the combustion gasses available for pressurization of joint free volumes. This will likely preclude any un-desirable molten slag deposition on seals or housing structures. During the numerous CFR tests, alumina / carbon deposition was always found on outboard surfaces of the rope.

3. CFR permeability had to be adjusted to account for initial squeeze. This effect is likely caused by the mechanical deformation of the CFR and resultant changes to the porous microstructure of the rope. Observed rope $\Delta p$'s were on the order of 200-300 psi per rope for the minimum gap cases and decreased <60 psi for the larger gaps

4. CFR permeability is affected to some extent by the in-situ deposition of alumina and/or other condensables in the combustion gas as the joint pressurizes. This increases the $\Delta p$'s across the rope during the later portion of the fill transient slightly increasing the fill times for the joint.

5. For the dual rope cases, CFR surface temperatures on the outboard side vary from 300-1100°F depending on the local gap. CFR surface temperature on the inboard side increase < 20°F for all cases with the gas in near thermal equilibrium with the solid carbon fibers. This outcome suggests that the CFR design provides more than sufficient thermal mass for quenching combustion gasses available for pressurization of the joint.

6. Large assembly gap joints will inherently have more free volume, higher peak flow rates and transfer less heat into the gap walls. As a result, both gas and CFR temperatures are significantly hotter on the outboard side of the barrier. Inboard of the CFRs, gas temperatures are relatively insensitive to initial gap.

7. For cases analyzed in this study where the CFRs remain fully seated and intact, predicted temperature rise in the metal housings was negligible. Primary seal pressurization environment will be thermally benign. There will be some irreversible recovery of gas temperature as the flow stagnates in dead ended regions of the joint but this effect will have no thermal impact on the structure.

References

1. RSRM Nozzle Joints Thermal Assessment, ED61, Memo ED63 (43-96), Marshall Space Flight Center, 1996

2. SINDA/JPR, "Joint Pressurization Routine (JPR) Theoretical Development and Users Manual", J. Louie Clayton, Memo ED66 (95-01), 1995

3. Systems Improved Numerical Differencing Analyzer (SINDA), JD Gaski, Network Analysis Associates Inc., 1987

4. O-Ring2: Volume Filling And O-ring Erosion Prediction Code, Improved Model Descriptions And Validation, Michael O'Malley, TWR-17030, August 1987

5. SRM Thermochemical Data, TP-H1148 Propellant, R. H. Whitesides, SRS Technologies, July 30, 1986

6. Carbon Fiber Rope (CFR) Joint Environment Simulator, A. Prince, Thiokol Corporation, ETP-1859, 1999